# Disruption of Interdomain Interactions via Partial Calcium Occupancy of Calmodulin†

Curt B. Boschek, Thomas C. Squier, and Diana J. Bigelow*

*Cell Biology and Biochemistry Group, Biological Sciences Division, Pacific Northwest National Laboratory, Richland, Washington 99352*

*Received December 11, 2006; Revised Manuscript Received January 22, 2007*

ABSTRACT: Binding of calcium to CaM exposes clefts in both N- and C-domains to promote their cooperative association with a diverse array of target proteins, functioning to relay the calcium signal regulating cellular metabolism. To clarify relationships between the calcium-dependent activation of individual domains and interdomain structural transitions associated with productive binding to target proteins, we have utilized three engineered CaM mutants that were covalently labeled with *N*-(1-pyrene) maleimide at introduced cysteines in the C- and N-domains, i.e., T110C ($Py_C$-CaM), T34C ($Py_N$-CaM), and T34C/T110C ($Py_2$-CaM). These sites were designed to detect known conformers of CaM such that upon association with classical CaM-binding sequences, the pyrenes in $Py_2$-CaM are brought close together, resulting in excimer formation. Complementary measurements of calcium-dependent enhancements of monomer fluorescence of $Py_C$-CaM and $Py_N$-CaM permit a determination of the calcium-dependent activation of individual domains and indicate the sequential calcium occupancy of the C- and N-terminal domains, with full saturation at 7.0 and 300 $\mu$M calcium, respectively. Substantial amounts of excimer formation are observed for apo-CaM prior to peptide association, indicating that interdomain interactions occur in solution. Calcium binding results in a large and highly cooperative reduction in the level of excimer formation; its calcium dependence coincides with the occupancy of C-terminal sites. These results indicate that interdomain interactions between the opposing domains of CaM occur in solution and that the occupancy of C-terminal calcium binding sites is necessary for the structural coupling between the opposing domains associated with the stabilization of the interdomain linker to enhance target protein binding.

Calmodulin (CaM)[1] represents the primary calcium sensor in all eukaryotic cells, functioning to interpret the calcium signal to modulate the activities of more than 50 different target proteins to affect cellular metabolism in response to extracellular signals (*1*). CaM consists of two globular domains separated by a central linker sequence (i.e., $Met^{76}$−$Ser^{81}$) (Figure 1). Elevations in the level of intracellular calcium promote occupancy of pairs of EF-hand sites on both the C- and N-terminal domains of CaM and function to induce global structural changes within each domain which stabilizes a structure of CaM capable of binding to target proteins (*2*−*6*). Following calcium activation, CaM binds to a diverse set of target proteins through association with both globular domains, which normally involves the initial association between the C-terminal domain of CaM and the CaM-binding sequence of the target protein, followed by the structural collapse and binding of the amino-terminal domain (*7*−*11*). The C-terminal domain cooperatively binds calcium with high affinity (*12*−*14*), while the lower calcium affinity of the N-terminal domain may contribute to the ordered binding of CaM associated with the productive activation of many target proteins. Differences in calcium affinities of the C- and N-terminal domains suggest that under some conditions CaM may exist in a partially activated state involving, for example, two bound calcium ions that promote a nonproductive association of CaM which facilitates the rapid modulation of target protein function upon full calcium activation (*15*, *16*).

Multiple high-resolution structures of apo and calcium-activated CaM suggest the presence of considerable structural heterogeneity with respect to both the interhelical angles within each globular domain and in the proximity and structural coupling between the opposing domains (*3*, *17*−*19*). In addition to the initially characterized structure of calcium-activated CaM in which the opposing domains are

† This work was supported by NIH Grants AG12993 and AG18013. Battelle is operated for the U.S. Department of Energy under Contract DE-AC05-76RL0 1830.

* To whom correspondence should be addressed: Cell Biology and Biochemistry Group, 790 6th St., Mail Stop P7-53, Pacific Northwest National Laboratory, Richland, WA 99354. Telephone: (509) 376-2378. Fax: (509) 376-6767. E-mail: diana.bigelow@pnl.gov.

[1] Abbreviations: $\beta$-ME, 2-mercaptoethanol; CaM, calmodulin; EGTA, ethylene glycol bis(2-aminoethyl ether)-*N*,*N*,*N*′,*N*′-tetraacetic acid; DTT, dithiothreitol; ESI-MS, electrospray ionization mass spectrometery; HEPES, *N*-(2-hydroxyethyl)piperazine-*N*′-2-ethanesulfonic acid; IPTG, $\beta$-D-1-thiogalactopyranoside; M13, peptide corresponding to the calmodulin-binding sequence $K^{577}$RRWKKNFIAVSAANRFKKISSSGAL$^{602}$ of skeletal MLCK; MLCK, myosin light chain kinase; MS, mass spectrometry; PDE, cyclic nucleotide phosphodiesterase; Py, pyrene; $Py_N$-CaM, *N*-(1-pyrene) maleimide-labeled T34C CaM; $Py_C$-CaM, *N*-(1-pyrene) maleimide-labeled T110C CaM; $Py_2$-CaM, T34C/T110C CaM labeled at both introduced cysteines with *N*-(1-pyrene) maleimide; SDS−PAGE, sodium dodecyl sulfate−polyacrylamide gel electrophoresis; TCEP, tris(carboxyethyl)phosphine.

10.1021/bi6025402 CCC: $37.00 
Published on Web 03/23/2007

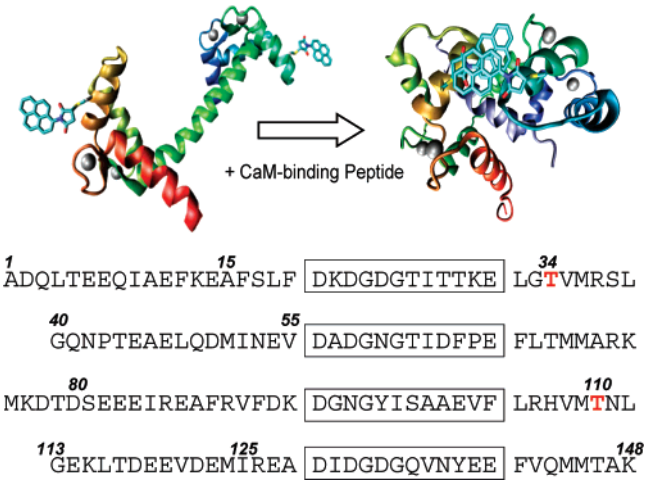


FIGURE 1: Design of CaM mutants to facilitate interdomain excimer formation. The top panel is a schematic representation of $Py_2$-CaM with pyrenes bound at T34C within the N-terminal domain (red) and at T110C within the C-terminal domain (blue); bound calcium ions are depicted as gray spheres. CaM structures were generated with VMD version 1.8.2 (*67*) and rendered with POV-ray version 3.5 (www.povray.org) for calcium-activated CaM (PDB entry 3cln) or CaM bound to M13 (PDB entry 2bbm). The bottom panel is the amino acid sequence of CaM indicating positions of cysteines (red); the four calcium-binding sequences are aligned and boxed.

widely separated in an extended structure (*20*, *21*), collapsed structures suggest that both domains may come close together (*18*). Indeed, the activated form of yeast CaM, which lacks calcium binding site 4, exists in a collapsed structure (*22*), suggesting that calcium occupancy may modulate the spatial separation between the opposing domains of CaM. However, while molecular dynamics simulations have suggested that CaM may undergo large amplitude structural changes prior to association with the CaM-binding sequences of target proteins (*23*), there are currently no reports demonstrating a direct association between the opposing domains of CaM in solution prior to association with target proteins or how partial occupancy of calcium binding sites affects the spatial relationship between the opposing domains of CaM.

To identify possible interdomain interactions between the opposing domains of CaM, we have labeled introduced cysteines located on the opposing domains of CaM using the small, environmentally sensitive fluorescent probe *N*-(1-pyrene) maleimide (*24*). Thus, upon labeling of the single cysteine in the C-domain (T110C, $Py_C$-CaM) or in the N-domain (T34C, $Py_N$-CaM), fluorescence spectroscopy can be used to assess the calcium-dependent activation of the individual domains of CaM. By comparison, when both domains are labeled with *N*-(1-pyrene) maleimide in the CaM T34C/T110C mutant ($Py_2$-CaM), interdomain interactions can be detected through the formation of excited-state dimers (excimers), resulting from contact interactions between the pyrenes covalently bound to the opposing domains. Importantly, the emission maximum of the excimer is red-shifted and is easily distinguished from monomer fluorescence emission (*25*), permitting local conformational changes to be readily discriminated from interdomain interactions. We report, for the first time, interdomain contact interactions between the opposing domains of CaM that result in excimer formation, which are disrupted by calcium activation. Using fluorescence spectroscopy, we are able to independently assess the sequential calcium-dependent activation of the C- and N-terminal domains of CaM, where the half-points associated with calcium activation are $1.16 \pm 0.04$ and $5.2 \pm 0.6$ $\mu$M, respectively. A highly cooperative disruption of the interdomain contact interaction between the opposing domains of CaM is co-incident with calcium occupancy of C-terminal calcium binding sites. These results indicate a structural coupling between the opposing domains of CaM that is mediated by the calcium-dependent activation of the C-terminal domain. In the activated state, the opposing domains are free to undergo high-affinity and cooperative binding to CaM-dependent target proteins.

## EXPERIMENTAL PROCEDURES

*Materials.* *N*-(1-Pyrene) maleimide, *N*-(1-pyrene) iodoacetamide, and the calcium-sensitive dyes Fura-2, Fura-4, and Fura-6 were obtained from Invitrogen/Molecular Probes (Eugene, OR). The synthetic peptide M13 (KRRWKKNFIAVSAANRFKKISSSGAL), corresponding to the calmodulin-binding domain (residues 577−602) of skeletal muscle myosin light chain kinase (skMLCK), was purchased from Anaspec Labs (San Jose, CA). Adenosine deaminase and alkaline phosphatase were from Roche Diagnostics (Indianapolis, IN). Bovine heart cyclic nucleotide phosphodiesterase (PDE), *N*-(2-hydroxyethyl)piperazine-*N*′-2-ethanesulfonic acid (HEPES), tris(carboxyethyl)phosphine (TCEP), potassium iodide (KI), and cAMP were obtained from Sigma (St. Louis, MO). 2-Mercaptoethanol ($\beta$-ME) was obtained from Aldrich (Milwaukee, WI). All other chemicals were the purest grade commercially available. *Escherichia coli* BL21(DE3) cells containing plasmids for CaM mutants containing either single cysteines in the N-domain (i.e., T34C) or C-domain (i.e., T110C) or two cysteines (i.e., T34C/T110C) were provided by R. Bieber-Urbauer (*26*), and following induction with $\beta$-D-1-thiogalactopyranoside, CaM was purified essentially as previously described (*27*, *28*).

*Covalent Labeling of CaM with N-(1-Pyrene) Maleimide*. Prior to labeling, lyophilized CaM mutants (0.5 mg) containing either one ($Py_N$-CaM or $Py_C$-CaM) or two cysteines ($Py_2$-CaM) were dissolved in 0.5 mL of 50 mM HEPES (pH 7.3) and reduced with 0.25 $\mu$M tris(carboxyethyl)-phosphine (TCEP) for 2 h at room temperature, at which time a 20-fold molar excess of *N*-(1-pyrene) maleimide or *N*-(1-pyrene) iodoacetamide (1.2 mM) was slowly added and incubated with stirring in the dark for 2 h. Following concentration to 50 $\mu$L using a Microcon centrifugal concentrator with a 10 kDa molecular mass cutoff (Millipore Inc., Billerica, MA), excess dye was removed using a size exclusion Sephadex G25 column (0.8 g) expanded in 10 mM HEPES (pH 7.0) and poured into a 0.5 cm × 20 cm column. Separated *N*-(1-pyrene) maleimide-labeled CaM was routinely brought to 4 mL in 50 mM $NH_4HCO_3$ (pH 10) and stirred for 10 min in the dark to allow homogeneous hydrolysis of the maleimide ring that was required for observation of any excimer formation. Finally, the solution was concentrated and buffer exchanged using a Microcon centrifugal concentrator to a final volume of 0.5 mL in 50 mM HEPES (pH 7.3). The stoichiometry of bound pyrene was measured using an extinction coefficient ($\epsilon_{340}$) of 40 000 $M^{-1}$ $cm^{-1}$ (*29*). Identification of the extent of *N*-(1-pyrene) maleimide modification to CaM was further characterized using electrospray ionization mass spectrometry (ESI-MS) in positive ion mode, essentially as previously described (*30*)

and performed by the Mass Spectrometry Laboratory (University of Kansas, Lawrence, KS).

*Measurement of CaM Function*. The extent of CaM-dependent activation of phosphodiesterase (PDE) was measured to assess the function of wild-type and *N*-(1-pyrene) maleimide-labeled CaM mutants, essentially as previously described (*32*, *33*). Briefly, time-dependent changes in the absorbance at 265 nm were measured following the addition of 2.9 mM cAMP for PDE (0.003 unit/mL) in the presence of indicated amounts of CaM at 37 °C in 40 mM diglycine (pH 7.5), 2.1 mM $CaCl_2$, and 1.2 mM $MgSO_4$ in the presence of 4.0 units/mL adenosine deaminase and 30 units/mL alkaline phosphatase. The CaM concentration dependence of PDE activity was fit with the Hill equation.

*Determination of the Amount of Free Calcium*. Free calcium concentrations were estimated using MaxChelator (*34*) and were verified using the ratiometric calcium-sensitive dyes Fura-2, Fura-4, and Fura-6 whose dissociation constants for calcium were 0.14, 0.17, and 5.3 $\mu$M, respectively, essentially as previously described (*29*, *35*, *36*).

*Steady-State Fluorescence Measurements*. Spectra were acquired at 25 °C using a FluoroLog2 Spex instrument (Edison, NJ) at 1 nm resolution with both excitation and emission slits set at 5 nm with an integration time of 0.1 s, using an excitation wavelength of 320 nm. In all cases, samples consisted of CaM (40 nM) in 50 mM MOPS (pH 7.0), 0.1 M KCl, 1 mM $MgCl_2$, 1 mM EGTA, and sufficient calcium to yield the desired free calcium levels. Pyrene fluorescence peaks were deconvoluted to separate monomer from excimer fluorescence using the Peak Fitting Module (PFM) of OriginPro version 7.5 (OrginLab Corp., Northhampton, MA).

*Calcium Binding Affinities in CaM*. Changes in fluorescence intensities were used to assess the binding of calcium to both the N- and C-domains in $Py_N$-CaM and $Py_C$-CaM and were fit using the Hill equation:

$$Y = \frac{[Ca^{2+}]^n}{K^n + [Ca^{2+}]^n} \quad (1)$$

where $n$ is the Hill coefficient and $K$ is the macroscopic dissociation constant, which represents the sum of the microscopic equilibrium binding constants (i.e., $k_1 + k_2$) for homotropic cooperativity (*37*), where individual calcium binding sites (on either domain) are sequentially occupied by calcium:

$$CaM + Ca \overset{k_1}{\leftrightarrow} CaM{-}Ca + Ca \overset{k_2}{\leftrightarrow} CaM{-}Ca_2 \quad (2)$$

Further consideration of the mechanism underlying cooperative binding is possible, where

$$Y = \frac{K_1[Ca^{2+}] + 2K_2[Ca^{2+}]^2}{2(1 + K_1[Ca^{2+}] + K_2[Ca^{2+}]^2)} \quad (3)$$

The macroscopic equilibrium association constant $K_1$ corresponds to the sum of the two intrinsic equilibrium constants ($k_1$ and $k_2$) associated with binding of calcium to CaM, and $K_2$ corresponds to the product of the equilibrium constants associated with binding to both sites and includes contributions associated with cooperativity (i.e., $k_1k_2k_{12}$) (*36*). A lower estimate of the contribution of the cooperative interaction is possible assuming that $k_1 = k_2$:

$$K_c = \frac{4K_2}{K_1^2} \quad (4)$$

## RESULTS

*Labeling of CaM with N-(1-Pyrene) Maleimide*. To probe structural changes within the individual N- and C-terminal globular domains, two single-cysteine CaM mutants were specifically labeled with *N*-(1-pyrene) maleimide at introduced cysteines T34C and T110C in the N- and C-terminal domains of CaM (Figure 1) and designated $Py_N$-CaM and $Py_C$-CaM, respectively. To assess interdomain interactions, an additional double-cysteine CaM mutant (T34C/T110C) was labeled with *N*-(1-pyrene) maleimide, designated $Py_2$-CaM. $Pyr_2$-CaM permits the detection of CaM conformers in which the globular domains come into sufficient proximity for the physical stacking of pyrene rings, and this, in turn, results in excited-state dimer formation with the concomitant appearance of excimer fluorescence centered at 485 nm and red-shifted relative to the monomer fluorescence [centered at 395 nm (*25*)]. From the extinction coefficients of the bound dye, the respective stoichiometries of labeling for $Py_N$-CaM, $Py_C$-CaM, and $Py_2$-CaM were determined to be 1.0 ± 0.2, 1.1 ± 0.1, and 2.2 ± 0.3 pyrenes bound per CaM, respectively. The complete labeling of the unique cysteines in $Py_N$-CaM and $Py_C$-CaM was verified using ESI-MS (Figure 2). The major peak at 17 023 Da for $Py_N$-CaM and $Py_C$-CaM is consistent with the theoretical mass (17 023 Da), as previously described (*38*). No spectral intensity associated with unlabeled CaM (16 708 Da) is detected for either $Py_N$-CaM or $Py_C$-CaM samples, indicating the stoichiometric labeling of CaM with *N*-(1-pyrene) maleimide. $Py_2$-CaM is nonionizable and was not detected using mass spectrometry, consistent with prior observations (*39*).

*Retention of Function in Mutant and Derivatized CaM*. Following mutagenesis and covalent attachment of *N*-(1-pyrene) maleimide at T34C in $Py_N$-CaM, T110C in $Py_C$-CaM, or at both sites in $Py_2$-CaM, we have assessed the function of CaM through a consideration of the CaM-dependent activation of phosphodiesterase (PDE), which has previously been shown to be strongly dependent on CaM binding for activation (*40*). In comparison to the basal activity, there is a greater than 5-fold increase in PDE activity upon addition of saturating amounts of CaM (Figure 2). Neither the threonine to cysteine mutations nor their derivatization with *N*-(1-pyrene) maleimide significantly affects the CaM-dependent activation of PDE (Table 1). These results are in contrast with earlier measurements in which mutations that induce interdomain interactions result in large shifts in the CaM dependence of target protein activation (*28*) and indicate that pyrene-labeled CaM mutants remain fully functional and provide reliable indicators of conformational changes associated with the calcium-dependent activation of CaM.

*Interdomain Interactions for CaM in Solution.* In addition to the major fluorescence peak associated with the monomeric form of pyrene centered at 385 nm, the apo form of $Py_2$-CaM exhibits substantial excimer formation with a peak centered at 485 nm that represents 47% of the total integrated

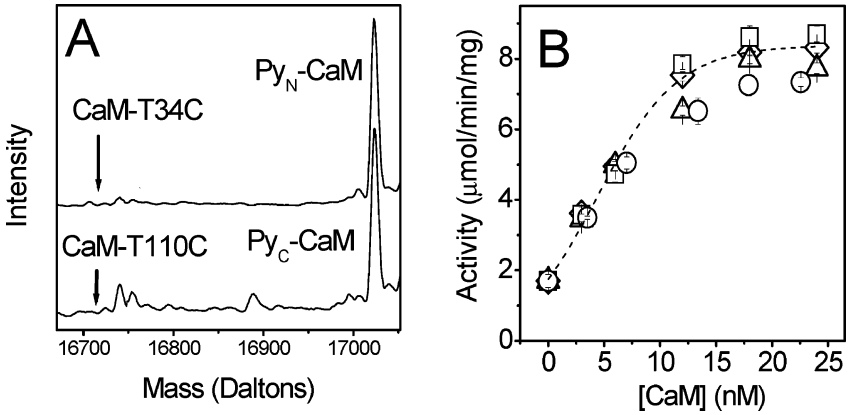


FIGURE 2: Retention of CaM function following mutagenesis and covalent labeling with *N*-(1-pyrene) maleimide. Whole protein electrospray ionization mass spectra (ESI-MS) (A) and functional activation of PDE (B) for wild-type CaM (◇), Py$_N$-CaM (△), Py$_C$-CaM (□), and Py$_2$-CaM (○). The observed mass of Py$_N$-CaM or Py$_C$-CaM is 17 023 Da, in agreement with the theoretical value (*38*). Masses of unlabeled T34C CaM or T110C CaM (16 708 Da) are indicated with arrows. PDE activity was measured as described in Experimental Procedures. Symbols and standard errors of the means are indicated for three independent measurements, and fitting parameters are summarized in Table 1.

Table 1: CaM-Dependent Activation of Phosphodiesterase[a]

| | $V_{max}$ ($\mu$mol mg$^{-1}$ min$^{-1}$) | [CaM]$_{1/2}$ (nM) |
|---|---|---|
| wild-type CaM | 8.3 ± 0.1 | 4.4 ± 0.3 |
| Py$_N$-CaM | 8.2 ± 0.4 | 4.9 ± 0.8 |
| Py$_C$-CaM | 9.0 ± 0.2 | 5.1 ± 0.4 |
| Py$_2$-CaM | 7.6 ± 0.4 | 5.7 ± 1.4 |

[a] Parameters from fits of the data presented in Figure 2B, fit to the Hill equation, where the Hill coefficient (*n*) is 1.0; maximal velocities ($V_{max}$) and CaM concentrations at half-maximal velocity, i.e., [CaM]$_{1/2}$, are also given.

intensity of the emission spectrum (Figure 3). Under the same conditions, no excimer formation is observed for CaM mutants that contain a single covalently bound pyrene chromophore, i.e., Py$_N$-CaM and Py$_C$-CaM, or an equimolar concentration of both constructs (data not shown). Thus, the excimer fluorescence observed for Py$_2$-CaM is a result of the intramolecular stacking of pyrene chromophores bound to opposing domains of CaM, rather than interactions between pyrenes bound to different CaM molecules. Moreover, accommodation of the pyrene stacking interactions (optimal orientation and proximity) leading to excimer fluorescence requires conformational flexibility of the pyrenes with respect to the protein backbone which was provided by hydrolysis of the maleimide ring; in addition, a lesser degree of pyrene excimer fluorescence was observed when the iodoacetamide linker was used (Figure S1 of the Supporting Information).

At micromolar concentrations of calcium, there is a significant decrease in the intensity of the excimer peak, indicating that calcium binding disrupts interdomain interactions between the N- and C-domains of CaM (Figure 3). The presence of residual excimer formation following calcium activation is consistent with some high-resolution structures of CaM that indicate a physical proximity between the N- and C-domains (*18*), but suggest that following calcium activation these are minor conformers. From a consideration of the calcium concentration dependence of the integrated area of the excimer fluorescence alone or normalized by the monomer fluorescence changes (excimer to monomer ratio), it is apparent that there is a highly cooperative decrease in the level of excimer formation over the same narrow range of calcium concentrations normally associated with CaM

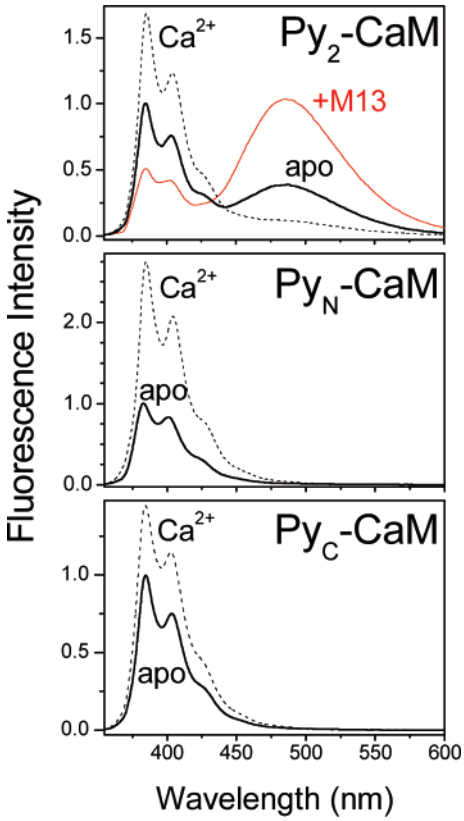


FIGURE 3: Calcium-dependent structural transitions. Fluorescence spectra of apo-CaM (solid black line) and calcium-activated CaM alone (dashed line) or bound to M13 peptide (red line) for Py$_2$-CaM (top), Py$_C$-CaM (middle), and Py$_N$-CaM (bottom). Spectra were collected at 25 °C for samples of 40 nM CaM in 50 mM MOPS (pH 7.0), 0.1 M KCl, 1 mM $MgCl_2$, and 1 mM EGTA in the presence of sufficient calcium for free calcium concentrations of either 5 nM (apo-CaM) or 700 $\mu$M (calcium-saturated CaM); when indicated, 60 nM M13 peptide was included. Spectral intensities are normalized to that of apo-CaM in each case.

activation (Figure 4 and Figure S2 of the Supporting Information), where the macroscopic dissociation constant is ~2.1 ± 0.2 $\mu$M and the Hill coefficient is 2.2 ± 0.3 (Table 2).

*Excimer Fluorescence following Peptide Binding*. To appreciate the fraction of apo-CaM conformers in which

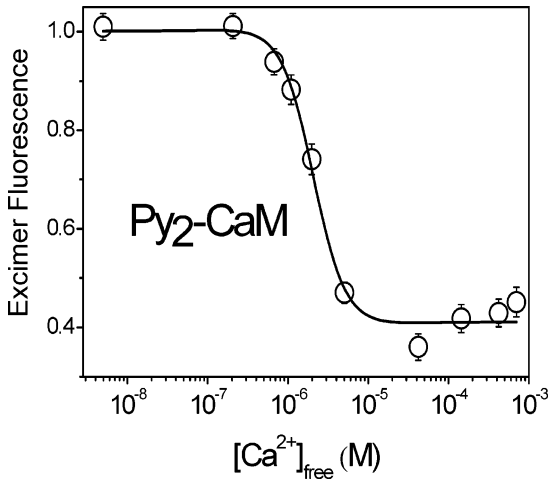


FIGURE 4: Calcium-dependent disruption of interdomain interactions. Calcium concentration-dependent decrease in the excimer fluorescence of $Py_2$-CaM, where symbols and standard errors of the mean are for three independent measurements. Experimental conditions are as described in the legend of Figure 3, where sufficient calcium was added to result in each specified free calcium level. Excitation was at 320 nm, and fluorescence emission was measured from the integrated intensity associated with the excimer peak centered at 485 nm.

opposing domains are sufficiently close for the emission of excimer fluorescence, we have measured the amount of excimer formation of $Py_2$-CaM upon association with the CaM-binding sequence of skeletal muscle MLCK (i.e., M13), where the bound pyrenes are expected to be brought into proximity on the basis of the high-resolution crystal structure of the calcium-bound form of CaM complexed to the M13 peptide (*18*) (Figure 1). Indeed, in the crystal structure (i.e., PDB entry 2bbm) the α-carbons of T34 and T110 in CaM bound to M13 are separated by approximately 15 Å. Given the overall dimensions of the pyrene chromophore [i.e., 9.2 Å (*41*)], along with the fact that the bound CaM exists in a very narrow range of conformers (*42*), these results indicate that the excimer complex in this state represents an end point associated with strong interdomain coupling. Indeed, the excimer peak associated with $Py_2$-CaM bound to the M13 peptide corresponds to 84% of the total integrated spectral intensity. Given that the amount of excimer formation for apo-CaM in solution is approximately 56% of that observed for CaM bound to M13, and assuming that the compact conformation of CaM is highly stabilized by interaction with M13, this comparison suggests a substantial population of apo-CaM exists, at least transiently, in which the opposing domains of CaM are brought into proximity in a conformation that approximates that associated with peptide binding. Further, the smaller amount of excimer formation is consistent with prior measurements demonstrating calcium-dependent structural changes that affect the spatial separation between the opposing domains of CaM (*43*−*45*).

*Calcium-Dependent Activation of Individual Domains in CaM*. In addition to large changes in excimer formation resulting from stacking interactions between the pyrene rings ($\lambda_{max}$ = 485 nm), there are also substantial differences in the fluorescence associated with pyrene monomers ($\lambda_{max}$ = 385 nm) upon calcium binding that are indicative of conformational differences in each domain associated with calcium activation of CaM (Figure 3). Similar calcium-dependent changes in the monomer fluorescence are observed for $Py_N$- and $Py_C$-CaM, which increase by 2.5- and 1.6-fold, respectively, upon calcium activation. The larger increase in fluorescence for $Py_N$-CaM in comparison to that of $Py_C$-CaM is consistent with prior measurements indicating that there are larger structural rearrangements within the N-domain co-incident with calcium activation (*33*, *46*). From the calcium concentration dependence of the calcium activation of the individual domains of CaM, we observe cooperative increases in fluorescence (Figure 5 and Table 2). The respective calcium binding affinities are well separated with macroscopic dissociation constants obtained from fits using the Hill equation of 1.16 ± 0.04 and 5.2 ± 0.6 μM, consistent with the higher calcium binding affinity of the C-terminal domain relative to the N-terminal binding sites (*13*, *14*, *47*, *48*). Consistent with prior results, these measurements indicate the sequential calcium-dependent activation of the C- and N-terminal domains of CaM (*12*, *48*). Saturation of the C-terminal domain calcium binding sites coincides with disruption of excimer formation associated with interdomain interactions (Figures 4 and 5). In addition, at this calcium concentration, 50% of the total fluorescence change of $Py_N$-CaM has occurred. However, the cooperative calcium binding suggests that the N-terminal domain exists as a mixture of states consisting of the apo form and two calciums bound per domain, rather than as partially filled (one calcium per N-domain). Thus, the absence of additional changes in excimer formation at the higher calcium concentrations necessary for full activation of the N-terminal domain indicates that the disruption of excimer formation is dependent upon occupancy of both high-affinity calcium binding sites in the C-terminal domain.

## DISCUSSION

*Summary of Results*. For the first time, we have detected interdomain contact interactions between the opposing domains of CaM, the association of which is disrupted upon calcium activation (Figure 3). These measurements take advantage of three engineered CaM mutants that permit the selective attachment of a pyrene chromophore on either the N-terminal domain ($Py_N$-CaM), the C-terminal domain ($Py_C$-CaM), or both domains of CaM ($Py_2$-CaM) with full retention of function (Figure 2). In combination with fluorescence spectroscopy, these constructs permit a direct comparison between structural changes associated with the calcium-dependent activation of the N- and C-domains of CaM with structural transitions that modulate interdomain interactions. Calcium-dependent structural transitions measured from monomer fluorescence and associated with binding of calcium to the individual N- and C-domains are cooperative and widely separated, such that the free calcium concentration associated with activation of the individual domains is required to be 300 and 7 μM, respectively (Figure 5 and Table 2). In comparison with the structural changes associated with the individual domains, a highly cooperative disruption of interdomain interactions is induced by activation of the C-terminal domain of CaM (Figures 4 and 5). The partial occupancy of the N-terminal sites under these conditions implies that it is the calcium-dependent activation of the C-terminal domain that mediates structural coupling between the opposing domains of CaM (Figure 6). Thus, in the fully activated state, interactions between the opposing domains of CaM are minimized to permit these domains the

Table 2: Free Energies for Binding of Calcium to CaM[a]

| | $\Delta G_1$ (kcal/mol)[b] | $\Delta G_2$ (kcal/mol)[b] | $\Delta G_c$ (kcal/mol)[b] | $K_d$ ($\mu$M)[c] | $n$[c] |
|---|---|---|---|---|---|
| $Py_N$-CaM | $-7.3 \pm 0.1$ | $-14.2 \pm 0.1$ | $-0.42 \pm 0.05$ | $5.2 \pm 0.6$ | $1.4 \pm 0.2$ |
| $Py_C$-CaM | $-7.4 \pm 0.3$ | $-16.2 \pm 0.1$ | $-2.2 \pm 0.4$ | $1.2 \pm 0.1$ | $1.7 \pm 0.1$ |
| $Py_2$-CaM | $-6.8 \pm 0.4$ | $-15.4 \pm 0.1$ | $-2.6 \pm 0.7$ | $2.1 \pm 0.2$ | $2.2 \pm 0.3$ |

[a] Calcium binding was assessed by fitting the fluorescence changes of $Py_N$-CaM, $Py_C$-CaM, or $Py_2$-CaM, where the data are shown in Figure 5. [b] Gibbs free energies (in kilocalories per mole) are shown for fits of the data to eq 3 (Experimental Procedures). [c] Macroscopic dissociation constants ($K_d$) and Hill coefficients ($n$) obtained from fits of the data in Figure 5 to the Hill equation (eq 1) are given.

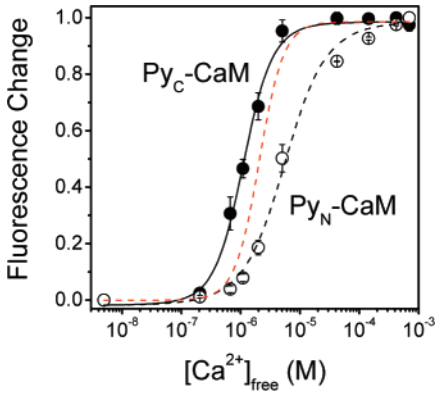


FIGURE 5: Calcium-dependent activation of individual domains. Calcium-dependent changes in the monomer fluorescence of $Py_N$-CaM (○) and $Py_C$-CaM (●) and associated nonlinear least-squares fit (see eq 1 in Experimental Procedures). Symbols and standard errors of the mean are from three independent measurements of the integrated intensities of the fluorescence spectra. Experimental conditions are as described in the legend of Figure 3, where sufficient calcium was added to result in each specified free calcium level. Excitation was at 320 nm, and the fluorescence emission was measured from the integrated intensity associated with the peak at 385 nm. For comparison, the normalized calcium-dependent loss of excimer fluorescence (dashed red line) taken from Figure 4 is shown.

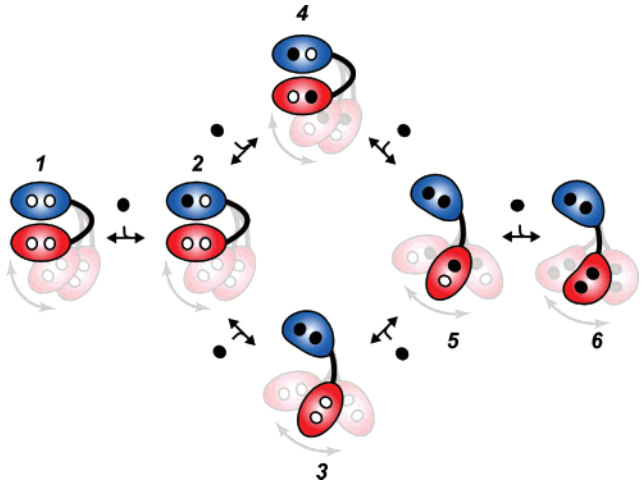


FIGURE 6: Structural coupling between the sequential occupancy of calcium-binding sites and interdomain interactions. The model depicts calcium-dependent conformational transitions involving intra- and interdomain changes that are associated with sequential binding of calcium to the C-domain (blue) and the N-domain (red) relative to the interdomain linker sequence ($Met^{76}$—$Ser^{81}$; line), where two calcium binding sites in each domain are indicated in the apo (○) or calcium-bound (●) form. The conformational heterogeneity of CaM conformers is indicated by multiple dark and faded structures. Each dark image indicates a structure detected by pyrene fluorescence changes. Faded images indicate additional suggested conformers based on observations that the pyrene excimer fluorescence of apo and Ca-bound states of CaM is a fraction of that of the peptide (M13)-bound state (Figure 3). Intermediate structures are numbered for reference.

freedom to undergo high-affinity and cooperative binding to target proteins.

*Calcium Activation and Interdomain Interactions*. Calcium ions bind to two pairs of EF-hand structures on the C- and N-domains of CaM to induce conformational changes within each domain that involve exposure of hydrophobic sequences through rigid body helical reorientations; these structural rearrangements are critical to the association of CaM with target proteins (*2*−*5*). The available structures of CaM in solution, using NMR, indicate considerable conformational heterogeneity and suggest that the individual domains within the calcium-activated state of CaM fluctuate between closed and open states prior to their association with target proteins (*49*). In addition, calcium-induced changes in the spatial arrangement between the opposing domains of CaM are mediated through the central linker sequence (i.e., $Met^{76}$—$Ser^{81}$), which has been suggested to be critical to the high-affinity binding of CaM to target proteins (*12*, *19*, *28*, *31*, *33*, *45*, *48*, *50*−*57*). Considerable heterogeneity has also been reported from available high-resolution crystal structures of calcium-activated CaM, which exists in both extended structures in which the opposing domains of CaM are well separated and in compact structures that bring the N- and C-domains of CaM into spatial proximity (*3*, *17*−*21*, *58*). Thus, these prior measurements would not have detected poorly populated and conformationally disordered states. Likewise, the current observation that interdomain interactions are enhanced in the apo form of CaM is consistent with prior measurements, including ours, that indicate calcium binding stabilizes the average structure of CaM to decrease both the average spatial separation and half-width of the distance distribution between sites on the N- and C-domains (*43*, *57*). Indeed, molecular dynamics simulations also suggest considerable conformational plasticity as well as the propensity of the extended structure of calcium-activated CaM to form a more collapsed structure (*46*, *59*).

Consistent with this reported structural heterogeneity, the observed pyrene excimer fluorescence indicates that a fraction, rather than all, of the total $Py_2$-CaM molecules adopt conformers in which there is close approximation between the opposing domains of CaM in both the apo and calcium-bound states as compared with the M13 peptide-bound state (Figure 3). When calcium binds, there is a dramatic decrease in the level of excimer formation, indicating the spatial rearrangement of the opposing domains of CaM. These latter results are consistent with prior biophysical measurements using spin-label EPR, optical spectroscopy, and NMR that all suggest calcium-dependent rearrangements through the stabilization of the central sequence that will weaken interdomain interactions (*44*, *45*, *50*, *60*).

*Partial Calcium Occupancy and Physiological Relevance*. Intermediary conformations of CaM in which only the

C-terminal domain is activated have been reported to be physiologically important in promoting binding to some target proteins, such as MLCK (*15*, *61*). In this respect, the large differences in the calcium binding affinities of the C- and N-terminal domains as measured from monomer fluorescence of $Py_N$- and $Py_C$-CaM have important consequences, since multiple species of calcium-activated CaM are expected in solution as indicated in the model in Figure 6 (*48*, *62*). Using *N*-(1-pyrene) maleimide at introduced cysteines T34C and T110C in the N- and C-terminal domains of CaM, we were able to measure cooperative structural changes associated with calcium binding (Figure 4 and Table 2). Half-points of calcium activation, as well as macroscopic binding constants associated with calcium activation, are comparable to prior measurements irrespective of whether the data were fit using the Hill equation or more mechanistic models that specifically take into account the presence of multiple high-affinity calcium binding sites, indicating the these CaM mutants accurately reflect calcium-dependent structural transitions associated with the activation of the individual domains of CaM (Table 2) (*36*, *54*). Comparable measurements using $Py_2$-CaM demonstrate interdomain interactions, which are disrupted upon activation of the C-terminal domain of CaM (Figure 5). Thus, these data in total indicate the following relationship between high-affinity calcium binding and the sequence of conformational events associated with CaM activation (Figure 6), in which the following states predominate. Apo-CaM (state 1), existing as a static or dynamic ensemble of compact to extended conformers, undergoes binding of one calcium ion to its C-domain (state 2). A second calcium ion preferentially binds to the second available site within the C-domain, inducing highly cooperative structural changes within the C-domain (to expose hydrophobic sites) with a simultaneous disruption of interdomain interactions (state 3). Finally, the third (state 5) and fourth (state 6) calcium ions bind cooperatively to the N-domain; full calcium occupancy of this domain is associated with conformational changes within the N-domain as indicated.

These results are consistent with earlier suggestions that calcium ion occupancy of the C-terminal domain of CaM is sufficient to promote association with CaM-binding sequences (*15*, *61*) and further suggest that the disruption of interdomain interactions is necessary for high-affinity target protein binding (*28*). In several cases, binding of CaM to CaM-binding sequences of target proteins enhances the binding of calcium to CaM, resulting in shifts in the amount of calcium necessary to fully saturate all four binding sites from approximately 300 $\mu$M for CaM alone to between 1 and 10 $\mu$M for CaM in the presence of target proteins, such as MLCK or the Ca-ATPase (*63*−*66*). Thus, it has been generally assumed that binding of CaM to CaM-dependent binding sequences is necessary for the observed increase in the calcium affinity of CaM into a more physiological range and that target binding is required for CaM to assume the activated conformation that promotes functional regulation of CaM targets. However, with the ability to differentiate calcium-dependent conformational changes within individual domains and given that binding of calcium to the C-domain and the disruption of interdomain interactions are observed at physiological calcium concentrations, our results indicate that CaM activation can occur in the absence of target protein binding.

*Conclusions and Future Directions.* We have demonstrated that occupancy of the C-terminal domain calcium binding sites in CaM disrupts interactions with the N-terminal domain of CaM and suggest that these global structural changes are part of the conformational switch for enhancing the ordered binding of CaM with target proteins so that the C-domain associates prior to the collapse of the N-domain necessary for target protein activation. Further, this intermediate state involving partial calcium occupancy may be important in the regulation of some target proteins, such as calcium channels, that are differentially regulated by the apo and calcium-bound states of CaM (*66*). Future measurements should be directed toward the definition of the transient kinetics associated with interdomain interactions in CaM both alone and in association with CaM-binding targets.

## ACKNOWLEDGMENT

We thank Todd D. Williams and Nadia Galeva of the Mass Spectrometry Lab (University of Kansas) for mass spectrometric analyses of CaM; we thank Natacha Lourette, Heather Smallwood, and Ljiljana Pasa-Tolic for helpful discussions.

## SUPPORTING INFORMATION AVAILABLE

Spectra demonstrating that greater probe flexibility is associated with increased excimer formation (Figure S1). Calcium activation of CaM disrupts excimer formation (Figure S2). This material is available free of charge via the Internet at http://pubs.acs.org.

## REFERENCES

1. Ikura, M., and Ames, J. B. (2006) Genetic polymorphism and protein conformational plasticity in the calmodulin superfamily: Two ways to promote multifunctionality, *Proc. Natl. Acad. Sci. U.S.A. 103*, 1159−1164.
2. LaPorte, D. C., Wierman, B. M., and Storm, D. R. (1980) Calcium-induced exposure of a hydrophobic surface on calmodulin, *Biochemistry 19*, 3814−3819.
3. Chou, J. J., Li, S., Klee, C. B., and Bax, A. (2001) Solution structure of $Ca^{2+}$-calmodulin reveals flexible hand-like properties of its domains, *Nat. Struct. Biol. 8*, 990−997.
4. Goto, K., Toyama, A., Takeuchi, H., Takayama, K., Saito, T., Iwamoto, M., Yeh, J. Z., and Narahashi, T. (2004) $Ca^{2+}$ binding sites in calmodulin and troponin C alter interhelical angle movements, *FEBS Lett. 561*, 51−57.
5. Yang, C., Jas, G. S., and Kuczera, K. (2004) Structure, dynamics and interaction with kinase targets: Computer simulations of calmodulin, *Biochim. Biophys. Acta 1697*, 289−300.
6. Vigil, D., Gallagher, S. C., Trewhella, J., and Garcia, A. E. (2001) Functional dynamics of the hydrophobic cleft in the N-domain of calmodulin, *Biophys. J. 80*, 2082−2092.
7. Sun, H., and Squier, T. C. (2000) Ordered and cooperative binding of opposing globular domains of calmodulin to the plasma membrane Ca-ATPase, *J. Biol. Chem. 275*, 1731−1738.
8. Persechini, A., McMillan, K., and Leakey, P. (1994) Activation of myosin light chain kinase and nitric oxide synthase activities by calmodulin fragments, *J. Biol. Chem. 269*, 16148−16154.
9. Crivici, A., and Ikura, M. (1995) Molecular and structural basis of target recognition by calmodulin, *Annu. Rev. Biophys. Biomol. Struct. 24*, 85−116.
10. Ehrhardt, M. R., Urbauer, J. L., and Wand, A. J. (1995) The energetics and dynamics of molecular recognition by calmodulin, *Biochemistry 34*, 2731−2738.
11. Kranz, J. K., Flynn, P. F., Fuentes, E. J., and Wand, A. J. (2002) Dissection of the pathway of molecular recognition by calmodulin, *Biochemistry 41*, 2599−2608.
12. VanScyoc, W. S., and Shea, M. A. (2001) Phenylalanine fluorescence studies of calcium binding to N-domain fragments of

*Paramecium* calmodulin mutants show increased calcium affinity correlates with increased disorder, *Protein Sci. 10*, 1758−1768.
13. Klevit, R. E., Dalgarno, D. C., Levine, B. A., and Williams, R. J. (1984) $^1$H-NMR studies of calmodulin. The nature of the $Ca^{2+}$-dependent conformational change, *Eur. J. Biochem. 139*, 109−114.
14. Kilhoffer, M. C., Kubina, M., Travers, F., and Haiech, J. (1992) Use of engineered proteins with internal tryptophan reporter groups and pertubation techniques to probe the mechanism of ligand-protein interactions: Investigation of the mechanism of calcium binding to calmodulin, *Biochemistry 31*, 8098−8106.
15. Heller, W. T., Krueger, J. K., and Trewhella, J. (2003) Further insights into calmodulin-myosin light chain kinase interaction from solution scattering and shape restoration, *Biochemistry 42*, 10579−10588.
16. Ehlers, M. D., and Augustine, G. J. (1999) Cell signalling. Calmodulin at the channel gate, *Nature 399*, 105, 107−108.
17. Wilson, M. A., and Brunger, A. T. (2000) The 1.0 Å crystal structure of $Ca^{2+}$-bound calmodulin: An analysis of disorder and implications for functionally relevant plasticity, *J. Mol. Biol. 301*, 1237−1256.
18. Fallon, J. L., and Quiocho, F. A. (2003) A closed compact structure of native $Ca^{2+}$-calmodulin, *Structure 11*, 1303−1307.
19. Jaren, O. R., Kranz, J. K., Sorensen, B. R., Wand, A. J., and Shea, M. A. (2002) Calcium-induced conformational switching of *Paramecium* calmodulin provides evidence for domain coupling, *Biochemistry 41*, 14158−14166.
20. Babu, Y. S., Sack, J. S., Greenhough, T. J., Bugg, C. E., Means, A. R., and Cook, W. J. (1985) Three-dimensional structure of calmodulin, *Nature 315*, 37−40.
21. Chattopadhyaya, R., Meador, W. E., Means, A. R., and Quiocho, F. A. (1992) Calmodulin structure refined at 1.7 Å resolution, *J. Mol. Biol. 228*, 1177−1192.
22. Starovasnik, M. A., Davis, T. N., and Klevit, R. E. (1993) Similarities and differences between yeast and vertebrate calmodulin: An examination of the calcium-binding and structural properties of calmodulin from the yeast *Saccharomyces cerevisiae*, *Biochemistry 32*, 3261−3270.
23. Vorherr, T., Kessler, O., Mark, A., and Carafoli, E. (1992) Construction and molecular dynamics simulation of calmodulin in the extended and in a bent conformation, *Eur. J. Biochem. 204*, 931−937.
24. Sastry, S., and Linderoth, N. (1999) Molecular mechanisms of peptide loading by the tumor rejection antigen/heat shock chaperone gp96 (GRP94), *J. Biol. Chem. 274*, 12023−12035.
25. Lehrer, S. S. (1997) Intramolecular pyrene excimer fluorescence: A probe of proximity and protein conformational change, *Methods Enzymol. 278*, 286−295.
26. Allen, M. W., Urbauer, R. J., Zaidi, A., Williams, T. D., Urbauer, J. L., and Johnson, C. K. (2004) Fluorescence labeling, purification, and immobilization of a double cysteine mutant calmodulin fusion protein for single-molecule experiments, *Anal. Biochem. 325*, 273−284.
27. Strasburg, G. M., Hogan, M., Birmachu, W., Thomas, D. D., and Louis, C. F. (1988) Site-specific derivatives of wheat germ calmodulin. Interactions with troponin and sarcoplasmic reticulum, *J. Biol. Chem. 263*, 542−548.
28. Yin, D., Sun, H., Ferrington, D. A., and Squier, T. C. (2000) Closer proximity between opposing domains of vertebrate calmodulin following deletion of $Met^{145}$−$Lys^{148}$, *Biochemistry 39*, 10255−10268.
29. Haugland, R. P., Ed. (2002) *Handbook of Fluorescent Probes and Research Products*, 9th ed., Molecular Probes, Inc., Eugene, OR.
30. Sacksteder, C. A., Whittier, J. E., Xiong, Y., Li, J., Galeva, N. A., Jacoby, M. E., Purvine, S. O., Williams, T. D., Rechsteiner, M. C., Bigelow, D. J., and Squier, T. C. (2006) Tertiary structural rearrangements upon oxidation of methionine 145 in calmodulin promotes targeted proteasomal degradation, *Biophys. J. 91*, 1480−1493.
31. Gao, J., Yin, D. H., Yao, Y., Sun, H., Qin, Z., Schoneich, C., Williams, T. D., and Squier, T. C. (1998) Loss of conformational stability in calmodulin upon methionine oxidation, *Biophys. J. 74*, 1115−1134.
32. Schiefer, S. (1986) Calmodulin, in *Methods of enzymatic analysis* (Bergmeyer, H. U., Bergmeyer, J., and Grable, M., Eds.) Vol. 9, VCH Publishers, Deerfield Beach, FL.
33. Chen, B., Mayer, M. U., Markillie, L. M., Stenoien, D. L., and Squier, T. C. (2005) Dynamic motion of helix A in the amino-terminal domain of calmodulin is stabilized upon calcium activation, *Biochemistry 44*, 905−914.
34. Patton, C., Thompson, S., and Epel, D. (2004) Some precautions in using chelators to buffer metals in biological solutions, *Cell Calcium 35*, 427−431.
35. Hunter, G. W., Negash, S., and Squier, T. C. (1999) Phosphatidylethanolamine modulates Ca-ATPase function and dynamics, *Biochemistry 38*, 1356−1364.
36. Pedigo, S., and Shea, M. A. (1995) Quantitative endoproteinase GluC footprinting of cooperative $Ca^{2+}$ binding to calmodulin: Proteolytic susceptibility of E31 and E87 indicates interdomain interactions, *Biochemistry 34*, 1179−1196.
37. Matthews, J. C. (1993) *Fundamentals of Receptor, Enzyme, and Transport Kinetics*, pp 50−54, CRC Press, Boca Raton, FL.
38. Osborn, K. D., Bartlett, R. K., Mandal, A., Zaidi, A., Urbauer, R. J., Urbauer, J. L., Galeva, N., Williams, T. D., and Johnson, C. K. (2004) Single-molecule dynamics reveal an altered conformation for the autoinhibitory domain of plasma membrane $Ca^{2+}$-ATPase bound to oxidatively modified calmodulin, *Biochemistry 43*, 12937−12944.
39. Jurva, U., Wikstrom, H. V., Weidolf, L., and Bruins, A. P. (2003) Comparison between electrochemistry/mass spectrometry and cytochrome P450 catalyzed oxidation reactions, *Rapid Commun. Mass Spectrom. 17*, 800−810.
40. Kakkar, R., Raju, R. V., and Sharma, R. K. (1999) Calmodulin-dependent cyclic nucleotide phosphodiesterase (PDE1), *Cell. Mol. Life Sci. 55*, 1164−1186.
41. Birks, J. B., Ed. (1970) *Photophysics of Aromatic Molecules*, Wiley-Interscience, London.
42. Yao, Y., and Squier, T. C. (1996) Variable conformation and dynamics of calmodulin complexed with peptides derived from the autoinhibitory domains of target proteins, *Biochemistry 35*, 6815−6827.
43. Yao, Y., Schoneich, C., and Squier, T. C. (1994) Resolution of structural changes associated with calcium activation of calmodulin using frequency domain fluorescence spectroscopy, *Biochemistry 33*, 7797−7810.
44. Sun, H., Yin, D., and Squier, T. C. (1999) Calcium-dependent structural coupling between opposing globular domains of calmodulin involves the central helix, *Biochemistry 38*, 12266−12279.
45. Qin, Z., and Squier, T. C. (2001) Calcium-dependent stabilization of the central sequence between Met(76) and Ser(81) in vertebrate calmodulin, *Biophys. J. 81*, 2908−2918.
46. Wriggers, W., Mehler, E., Pitici, F., Weinstein, H., and Schulten, K. (1998) Structure and dynamics of calmodulin in solution, *Biophys. J. 74*, 1622−1639.
47. Wang, C. L. (1985) A note on $Ca^{2+}$ binding to calmodulin, *Biochem. Biophys. Res. Commun. 130*, 426−430.
48. VanScyoc, W. S., Sorensen, B. R., Rusinova, E., Laws, W. R., Ross, J. B., and Shea, M. A. (2002) Calcium binding to calmodulin mutants monitored by domain-specific intrinsic phenylalanine and tyrosine fluorescence, *Biophys. J. 83*, 2767−2780.
49. Krueger, J. K., Bishop, N. A., Blumenthal, D. K., Zhi, G., Beckingham, K., Stull, J. T., and Trewhella, J. (1998) Calmodulin binding to myosin light chain kinase begins at substoichiometric $Ca^{2+}$ concentrations: A small-angle scattering study of binding and conformational transitions, *Biochemistry 37*, 17810−17817.
50. Sun, H., Yin, D., Coffeen, L. A., Shea, M. A., and Squier, T. C. (2001) Mutation of Tyr138 disrupts the structural coupling between the opposing domains in vertebrate calmodulin, *Biochemistry 40*, 9605−9617.
51. Faga, L. A., Sorensen, B. R., VanScyoc, W. S., and Shea, M. A. (2003) Basic interdomain boundary residues in calmodulin decrease calcium affinity of sites I and II by stabilizing helix-helix interactions, *Proteins 50*, 381−391.
52. Gao, J., Yao, Y., and Squier, T. C. (2001) Oxidatively modified calmodulin binds to the plasma membrane Ca-ATPase in a nonproductive and conformationally disordered complex, *Biophys. J. 80*, 1791−1801.
53. Shea, M. A., Verhoeven, A. S., and Pedigo, S. (1996) Calcium-induced interactions of calmodulin domains revealed by quantitative thrombin footprinting of Arg37 and Arg106, *Biochemistry 35*, 2943−2957.
54. Vanscyoc, W. S., Newman, R. A., Sorensen, B. R., and Shea, M. A. (2006) Calcium Binding to Calmodulin Mutants Having Domain-Specific Effects on the Regulation of Ion Channels, *Biochemistry 45*, 14311−14324.

55. Sorensen, B. R., Faga, L. A., Hultman, R., and Shea, M. A. (2002) An interdomain linker increases the thermostability and decreases the calcium affinity of the calmodulin N-domain, *Biochemistry 41*, 15−20.
56. Yao, Y., Yin, D., Jas, G. S., Kuczer, K., Williams, T. D., Schoneich, C., and Squier, T. C. (1996) Oxidative modification of a carboxyl-terminal vicinal methionine in calmodulin by hydrogen peroxide inhibits calmodulin-dependent activation of the plasma membrane Ca-ATPase, *Biochemistry 35*, 2767−2787.
57. Yin, D., Kuczera, K., and Squier, T. C. (2000) The sensitivity of carboxyl-terminal methionines in calmodulin isoforms to oxidation by $H_2O_2$ modulates the ability to activate the plasma membrane Ca-ATPase, *Chem. Res. Toxicol. 13*, 103−110.
58. Johnson, C. K., Osborn, K. D., Allen, M. W., and Slaughter, B. D. (2005) Single-molecule fluorescence spectroscopy: New probes of protein function and dynamics, *Physiology 20*, 10−14.
59. Shepherd, C. M., and Vogel, H. J. (2004) A molecular dynamics study of $Ca^{2+}$-calmodulin: Evidence of interdomain coupling and structural collapse on the nanosecond timescale, *Biophys. J. 87*, 780−791.
60. Chang, S. L., Szabo, A., and Tjandra, N. (2003) Temperature dependence of domain motions of calmodulin probed by NMR relaxation at multiple fields, *J. Am. Chem. Soc. 125*, 11379−11384.
61. Heidorn, D. B., Seeger, P. A., Rokop, S. E., Blumenthal, D. K., Means, A. R., Crespi, H., and Trewhella, J. (1989) Changes in the structure of calmodulin induced by a peptide based on the calmodulin-binding domain of myosin light chain kinase, *Biochemistry 28*, 6757−6764.
62. Linse, S., Helmersson, A., and Forsen, S. (1991) Calcium binding to calmodulin and its globular domains, *J. Biol. Chem. 266*, 8050−8054.
63. Persechini, A., Yano, K., and Stemmer, P. M. (2000) $Ca^{2+}$ binding and energy coupling in the calmodulin-myosin light chain kinase complex, *J. Biol. Chem. 275*, 4199−4204.
64. Gao, J., Yin, D., Yao, Y., Williams, T. D., and Squier, T. C. (1998) Progressive decline in the ability of calmodulin isolated from aged brain to activate the plasma membrane Ca-ATPase, *Biochemistry 37*, 9536−9548.
65. Niggli, V., Adunyah, E. S., Penniston, J. T., and Carafoli, E. (1981) Purified ($Ca^{2+}$-$Mg^{2+}$)-ATPase of the erythrocyte membrane. Reconstitution and effect of calmodulin and phospholipids, *J. Biol. Chem. 256*, 395−401.
66. Jurado, L. A., Chockalingam, P. S., and Jarrett, H. W. (1999) Apocalmodulin, *Physiol. Rev. 79*, 661−682.
67. Humphrey, W., Dalke, A., and Schulten, K. (1996) VMD: Visual molecular dynamics, *J. Mol. Graphics 14*, 27−38.

BI6025402